Steady-state simulation of the seawater greenhouse condenser

Abdulrahim Mohammed Al-Ismaili[1*], Edward Keith Weatherhead[2]

(1. *Department of Soils, Water and Agricultural Engineering, College of Agricultural and Marine Sciences, Sultan Qaboos University, Muscat, Oman, P.O.Box 34, P.Code 123*;
2. *Centre for Water Science, School of Applied Sciences, Cranfield University, United Kingdom*)

Abstract: This paper presents an integrated steady-state model simulating the condenser of a seawater greenhouse in Oman. The developed model is capable of predicting the outlet air temperature and humidity, the outlet seawater temperature and the condensation rate. Validation experiments showed a good conformity between the predicted and measured values within the calibration ranges at high and low air flowrates. The mean predictive error (*PE*) for the predicted condensation rate was 15.25 and 22.67 mL min^{-1} at high and low flowrates, respectively and the index of agreement (*IA*) was 0.96 and 0.98, respectively. The model also accurately predicted the outlet humidity ratio with *PE* values of –0.00006 and –0.00018 kg kg^{-1} for high and low air flowrates, respectively and *IA* values of 1.00 and 0.99, respectively. The model showed a small discrepancy between the measured and predicted outlet air temperature but yet with a *PE* value of 0.35°C and 2.44°C at high and low air flowrates, respectively and *IA* values of 0.92 and 0.86, respectively. This discrepancy was attributed greatly to inaccuracy related to measurements caused by the non-horizontal airflow pattern and less-likely due to inaccuracy related to the simulation. The accuracy of the model to predict the outlet seawater temperature was excellent with a *PE* of –0.33°C and –0.10°C for high and low air flowrates, respectively and *IA* values of 0.98 and 0.99, respectively. Model's accuracy was also evaluated using three additional statistical prediction indicators; coefficient of determination, mean absolute predictive error and root mean square error. It was found that all prediction indicators for high and low air flowrates were very good.

Keywords: humidification-dehumidification, seawater greenhouse, condenser, simulation

Citation: Al-Ismaili, A. M., and E. K. Weatherhead. 2018. Steady-state simulation of the seawater greenhouse condenser. Agricultural Engineering International: CIGR Journal, 20(2): 52–60.

1 Introduction

Integration of a condenser in a greenhouse structure is very unusual (Stanghellini and van Meurs, 1992) especially in arid climates where the ambient humidity is relatively low. However, a condensation unit is a primary component in a seawater greenhouse (SWGH) for the condensation of moisture from the air stream flowing inside the greenhouse. The SWGH is similar to conventional fan-pad evaporatively-cooled greenhouses, yet it has two additional components; a second humidifier and a condenser. The main objective of the SWGH is to provide a cheap freshwater source to irrigate cultivated crops inside the greenhouse where freshwater is not available, not accessible or not affordable. Four SWGHs have been built to date; the first greenhouse was in Spain in 1994 (Goosen et al., 2000; Light-Works, 2001), the second was in UAE in 2000 (Davies et al., 2004; Bourouni et al., 2011; Davies and Paton, 2006, 2005; Davies and Paton, 2004), the third was in Oman in 2004 (Al-Ismaili, 2009) and the forth was in South Australia in 2010 (ABC, 2012; Aljazeera-English, 2012). More details about SWGHs can be found in Al-Ismaili and Jayasuriya (2016).

Figure 1 illustrates the SWGH located in Muscat, Oman. In this greenhouse, seawater is used to wet the first humidifier (i.e. evaporative cooler) and then the seawater is pumped to the condenser as a coolant. As air flows from the first humidifier to the second humidifier, it gains more sensible and latent heat causing it to have a higher temperature and lower relative humidity. Seawater

Received date: 2017-09-14 **Accepted date:** 2018-01-30

*** Corresponding author: A. M. Al-Ismaili,** Department of Soils, Water and Agricultural Engineering, College of Agricultural and Marine Sciences, Sultan Qaboos University, Muscat, Oman. Email: abdrahim@squ.edu.om.

used in the second humidifier is pre-heated via a solar heater in order to increase air temperature (by convection) and humidity (by evaporation) before reaching the condenser. The success of the SWGH technology heavily relies on its effectiveness to produce freshwater, i.e. the effectiveness of the condensation unit (Alkhalidi et al., 2010; Zurigat et al., 2008; Dawoud et al., 2006; Ghaffour et al., 2015). Therefore, several attempts to predict the condensation rate using simulation models have been reported in literature. These models were developed using analytical and empirical approaches.

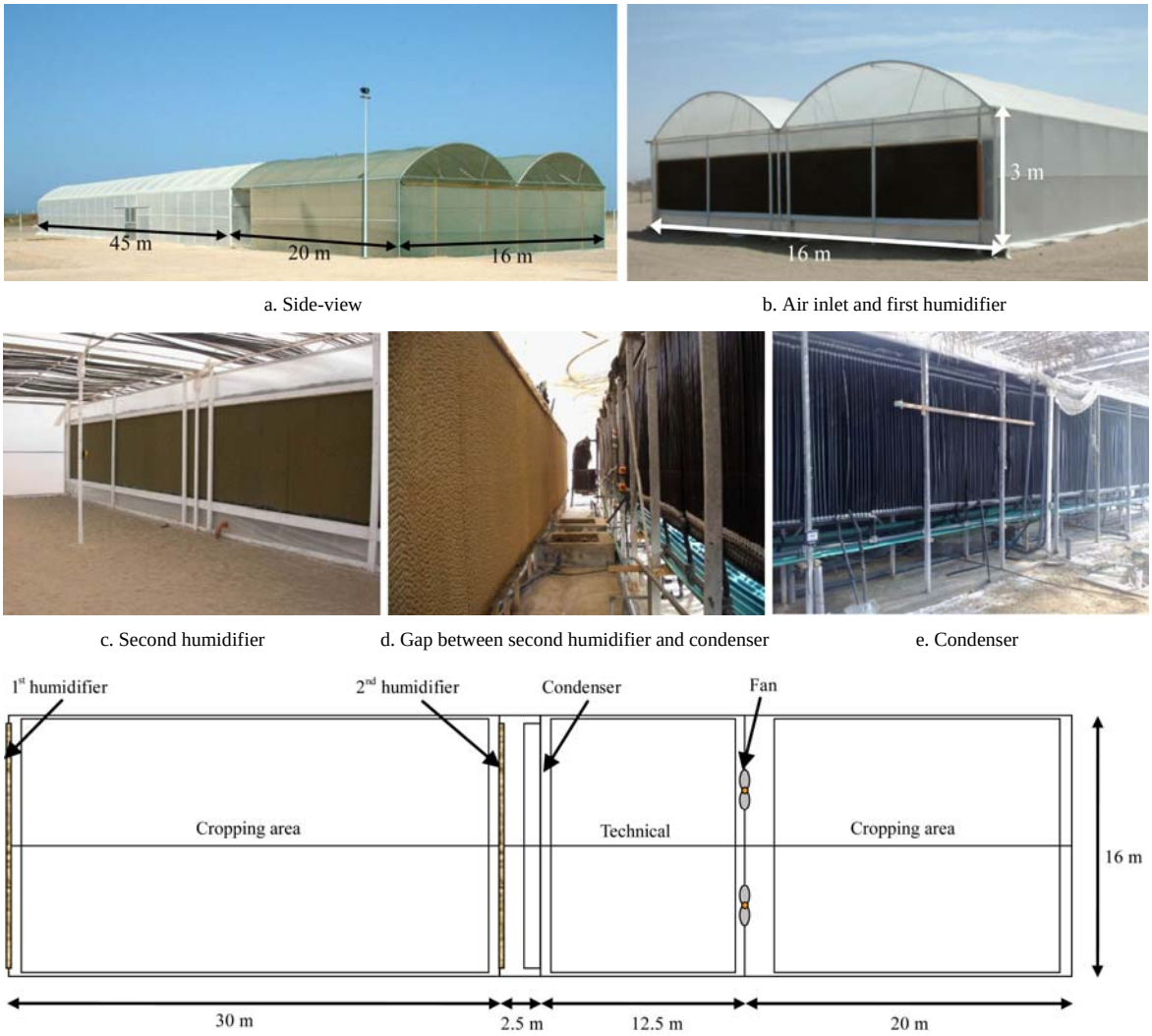

a. Side-view b. Air inlet and first humidifier

c. Second humidifier d. Gap between second humidifier and condenser e. Condenser

Figure 1 The SWGH in Oman (Direction of air flow is left to right throughout)

Most of the available studies followed the analytical approach to predict the condensation rate using heat and/or mass balance equations (Davies and Paton, 2006; Dawoud et al., 2006; Raoueche et al., 1996; Ghaffour et al., 2011; Goosen et al., 2003; Hajiamiri and Salehi, 2013; Quteishat et al., 2003; Sablani et al., 2003; Tahri et al., 2016; Zamen et al., 2013). This approach requires very detailed thermodynamic considerations and takes longer simulation time, yet it can be used for a wide range of design and operating variables. Tahri et al. (2009a, 2009b, 2010) reported that their heat balance model was capable of predicting the condensation rate with an accuracy ranging from 8% to 15%. The accuracy of this model was further improved by Douani et al. (2011). The empirical approach, on the other hand, has less complexity in development and takes less simulation time. However, their range of applications is limited to the range of input variables considered in the development of the model. Using a power-law regression technique, an empirical model predicting the condensation rate from the greenhouse width-length ratio was developed (Yetilmezsoy and Abdul-Wahab, 2014). However, the accuracy of this model was very low (Al-Ismaili and Jayasuriya, 2016). Yetilmezsoy and Abdul-Wahab (2014)

provided another empirical model estimating the condensation rate from the key input variables, namely, air temperature, humidity and flowrate and seawater temperature and flowrate. This model was found to be more accurate than the analytical model of Tahri et al. (2009b; 2010), yet less accurate than another analytical model (Tahri et al., 2013).

This study combines the analytical and empirical approaches in a steady-state model developed to predict not only the condensation rate but also the outlet air temperature and humidity and the outlet seawater temperature of the SWGH condenser in Oman. The accuracy of the model was evaluated by comparing the predicted variables with experimental data.

2 Condenser description

Figure 2 illustrates the condenser used in the SWGH in Oman. The condenser is 1.8 m high, 15 m wide and 0.8 m thick. It comprises 4832 vertical tubes arranged as 302 lines (across) of 16 rows (deep). The two fluids (air and seawater) flow in a cross-flow pattern through the condenser. The coolant enters the condenser through the last (rear) row of tubes and oscillates up and down in a direction opposing the flowing air until it leaves the condenser through the front row of tubes. The condenser tubes have a staggered arrangement where the transverse pitch (S_T) and diagonal pitch (S_D) are equal (Figure 2a and 2c). The tubes are made from polyvinylchloride (PVC) which is a salt-resistant material to avoid corrosion from the saline coolant fluid. To compensate for the poor thermal conductivity of PVC, the thickness of the tube walls is made very small (i.e. 240 micron) and the inlet coolant temperature is relatively low. Evaporatively-cooled seawater leaving the first humidifier could be used as a coolant if its temperature is sufficiently low (Lovichit et al., 2007). Al-Ismaili (2003) and Perret et al. (2005) monitored the temperature of water leaving the first humidifier in a pilot SWGH. They reported that the use of this water as a condenser coolant is feasible owing to its temperature being always below the dew-point temperature of the moist air passing through the condenser. Accordingly, this water was used as the coolant fluid in the SWGH in Oman.

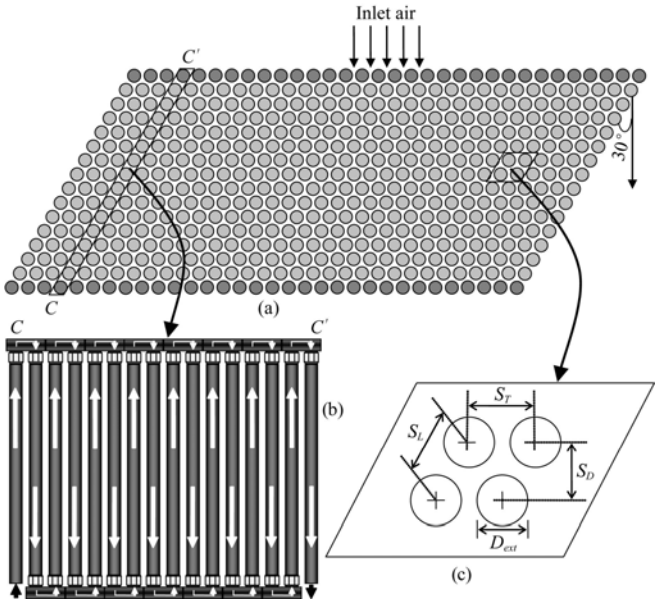

(a) a top view of air movement with respect to the staggered orientation of the condenser tubes, (b) side view of one line of connected tubes illustrating seawater movement through the condenser tubes and (c) some dimensional terms used in the development of the simulation model

Figure 2 Schematic of condenser used in the SWGH in Oman

3 Modeling

Figure 3 illustrates the inlet and outlet heat terms of the condenser. The following heat balance puts the inlet and outlet heat terms together:

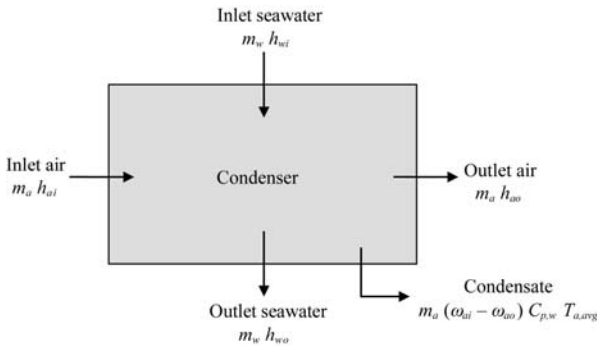

Figure 3 Schematic diagram illustrating the heat flows in the condenser

$$m_a[(h_{ai} - h_{ao}) - (\omega_{ai} - \omega_{ao})C_{P,w}\ T_{ao}] = m_w(h_{wo} - h_{wi}) \quad (1)$$

where the right side represents the overall heat transfer rate into the coolant water (Q_w) and the left side represents the overall heat transfer rate from the air (Q_a) including any condensed water, i.e. all sensible and latent heat lost from air will be gained by water (Zamen et al., 2013) assuming an adiabatic process. For this balance to stay valid, heat transfer taking place outside the tubes ($Q_{cv,ext}$), through the tube walls (Q_{cd}) and inside the tubes ($Q_{cv,int}$) must also be equal. Thus,

$$Q_a = Q_{cv,ext} = Q_{cd} = Q_{cv,\text{int}} = Q_w \quad (2)$$

The first and last terms can be solved as follows:

$$Q_a = [C_{p,da}(T_{ai} - T_{ao}) + \omega_{ai}(L_{v,0} + C_{p,wv}\ T_{ai}) - \omega_{ao}(L_{v,0} + C_{p,wv}\ T_{a,avg}) - (\omega_{ai} - \omega_{ao})\ C_{P,w}\ T_{a,avg}] \quad (3)$$

$$Q_w = m_w\ C_{p,w}\ (T_{wo} - T_{wi}) \quad (4)$$

Newton's law of cooling is used to estimate the external ($Q_{cv,ext}$) and internal ($Q_{cv,int}$) convective heat transfer rates:

$$Q_{cv,ext} = \left[\mathrm{Nu}_{ext}\frac{k_a}{D_{ext}}\right] A_{es}\left[\frac{T_{ai}+T_{ao}}{2} - T_{es}\right] \quad (5)$$

$$Q_{cv,int} = \left[\mathrm{Nu}_{int}\frac{k_w}{D_{int}}\right] A_{is}\left[T_{is} - \frac{T_{wi}+T_{wo}}{2}\right] \quad (6)$$

For $Q_{cv,ext}$, the average external Nusselt number (Nu_{ext}) in a staggered tube arrangement is calculated using Grimson's (1937) relation with Hausen's (1983) modifications:

$$\mathrm{Nu}_{ext} = 0.35 f_a\ \mathrm{Re}_{a,max}^{0.57}\ \mathrm{Pr}_a^{0.31} \quad (7)$$

Where the arrangement factor (f_a) in this relation is calculated as follows:

$$f_a = 1 + 0.1(S_T/D_{ext}) + 0.34(D_{ext}/S_L) \quad (8)$$

For $Q_{cv,int}$, the average internal Nusselt number (Nu_{int}) in a laminar flow (Re_w<50), assuming a constant wall temperature (T_{is}) and a fully-developed laminar flow, is calculated using the following relation (Hausen, 1983, 1943):

$$\mathrm{Nu}_{int} = 3.66 + \left[\frac{0.0668\ \frac{D_{int}}{L}\ \mathrm{Re}_w\ \mathrm{Pr}_w}{1 + 0.045\left(\frac{D_{int}}{L}\ \mathrm{Re}_w\ \mathrm{Pr}_w\right)^{2/3}}\right] \quad (9)$$

For Q_{cd}, Fourier's law of heat conduction is used:

$$Q_{cd} = \frac{2\pi\ k_{tube}\ H_{tube}\ (T_{es} - T_{is})}{\ln\left[\frac{D_{ext}}{D_{int}}\right]} \quad (10)$$

The input parameters in Equation (2)-(10) include the inlet air temperature (T_{ai}), inlet humidity ratio (ω_{ai}), air mass flowrate (m_a), inlet seawater temperature (T_{wi}) and seawater mass flowrate (m_w). These equations are solved simultaneously (iteratively) as illustrated in Figure 4 for generating the required outputs, i.e. T_{ao}, ω_{ao}, T_{wo} and R_c. However, it will not be possible to execute the simulation without assuming or estimating four output parameters. Therefore, initial values for T_{ao}, T_{es} and T_{wo} will be assumed but ω_{ao} will be estimated using the following relation:

$$R_c = 6.0\times10^4 m_a(\omega_{ai} - \omega_{ao}) \quad (11)$$

Where the numerical value 6.0x10^4 is used to maintain consistency of units.

The condensation rate (R_c) is estimated empirically from the influencing input parameters using multiple linear regression function in MS-Excel. Equation 11 will be also used to calculate the experimental ω_{ao} from measured R_c values.

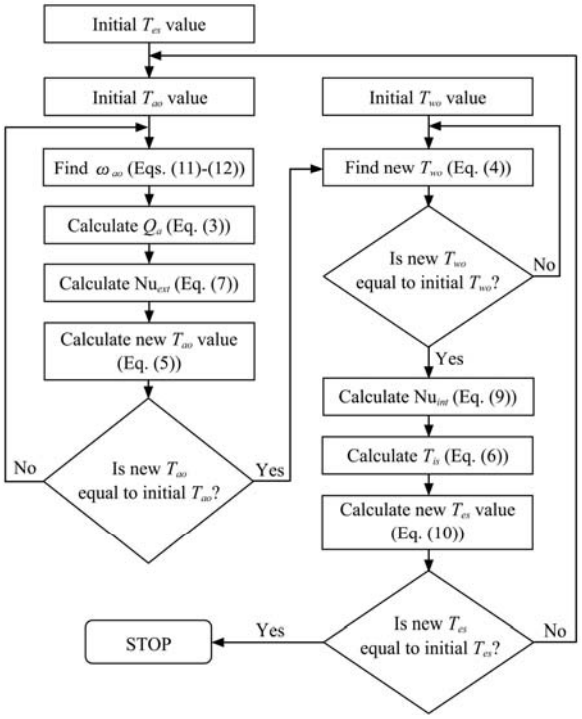

Figure 4 Flow diagram of the iterative procedure of the simulation model

4 Validation experiments

Validation experiments were carried out using the condenser of the SWGH in Oman during the summer months. In these experiments, the greenhouse setup and operational arrangements were kept unaltered. However, the effect of two air velocities on the condensation rate and other outlet variables was investigated. The two velocities were 0.14 m s^{-1} (Low air flowrate) and 0.27 m s^{-1} (High air flowrate). Table 1 gives the design and operational parameters of the condenser.

Inlet and outlet air temperatures and humidity were measured using Delta-T dual air temperature/humidity sensors (RHT2nl, Delta-T Devices Ltd., UK). Inlet and outlet coolant water temperatures were monitored using

Delta-T sealed temperature probes (BT1, Delta-T Devices Ltd., UK). A Delta-T tipping bucket gauge (RG1, Delta-T Devices Ltd., UK) was used to measure the condensation rate. Data from all sensors were retrieved and recorded at ten-minute intervals using a Delta-T datalogger (DL2e, Delta-T Devices Ltd., UK).

Table 1 Condenser design parameters used in the simulation

Parameter	Value
D_{ext} (m)	3.00×10^{-2}
D_{int} (m)	2.98×10^{-2}
H_{tube} (m)	1.81
S_T (m)	4.70×10^{-2}
S_D (m)	4.70×10^{-2}
S_L (m)	4.07×10^{-2}
Tube thickness (m)	2.40×10^{-4}
Number of rows	16
Number of columns	302
k_{tube} (W m^{-1} $^oC^{-1}$)	0.19

The accuracy of the model to predict T_{ao}, ω_{ao}, T_{wo} and R_c was compared against the measured values. Statistically, five indicators were used to evaluate the conformity of predicted values with experimental data. These indicators were the coefficient of determination (R^2), mean predictive error (*PE*), mean absolute predictive error (*AE*), root mean square error (*RMSE*) and index of agreement (*IA*). The predicted and measured values were also compared graphically.

5 Results and discussion

5.1 Condensation rate and humidity predictions

Equation (12) presents the empirical relation developed through multiple linear regression analysis to estimate the condensation rate (R_c) as a function of four input parameters. Large experimental data (971 datasets) were involved in the regression process and Table 2 provides the operating ranges of all parameters involved in the regression.

$$R_c = -237.25+57.04\ T_{ai}+40885.37\ \omega_{ai}+ 27.60\ m_a - 85.93\ T_{wi} \quad (R_c > 0) \tag{12}$$

The R^2 of this equation was 0.88 at a confidence level of 95%. When Equation (12) was used to estimate R_c for new datasets (which were not involved in the development of Equation (12)), it was found that the predicted and measured R_c values were in close conformity at high and low air flowrates (R^2 of 0.85 and 0.95, respectively). The model responded accurately to the changes in the inlet variables as clearly seen from Figure 5. The predicted and measured R_c at low air flowrate was much greater than predicted R_c at high air flowrate due to the increase in contact time between the moist air and the condenser tubes. It is clear from Table 3 that all five statistical prediction indicators for low and high air flowrates were very good. Therefore, the empirical relation (Equation (12)) can be confidently used to predict R_c for situations falling within the operating ranges of the input variables (Table 2).

Table 2 Operating ranges of experimental data involved in Equation (12)

Parameter	Experimental Rang
R_c (mL min^{-1})	0-1292.6
T_{ai} (^{o}C)	17.7-34.3
ω_{ai} (kg kg^{-1})	0.0119-0.0335
m_a (kg s^{-1})	2.1-4.4
T_{wi} (^{o}C)	15.2-7.5

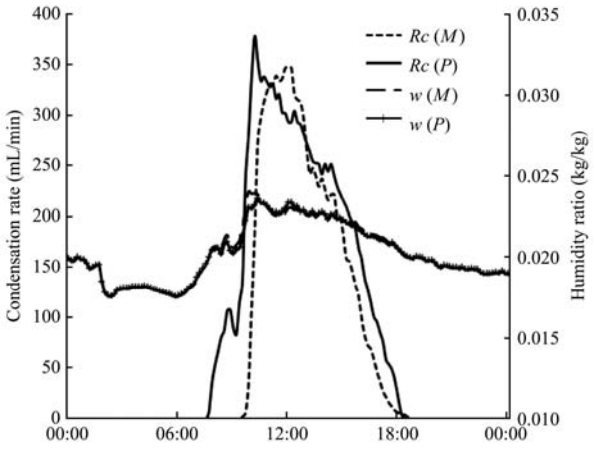

a. High air flowrate

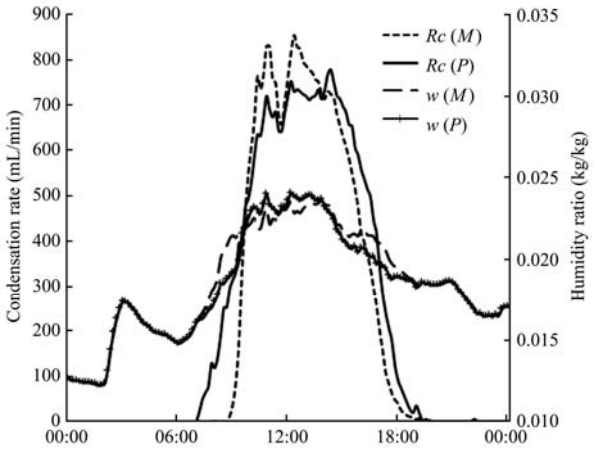

b. Low air flowrate

Figure 5 Measured (*M*) and predicted (*P*) condensation rate (*Rc*) and outlet humidity ratio (*w*) of the SWGH condenser at different air flowrate

The model also accurately predicted the outlet humidity ratio (ω_{ao}) with R^2 values of 0.99 and 0.96 for high and low air flowrates, respectively. Other prediction indicators showed excellent accuracy as clearly seen from Table 3. Figure 5 shows that the predicted and measured ω_{ao} were overlapping at most of the times.

Table 3 Statistical indicators of the predicted values at high and low air flowrates

Statistical Indicators	Equations*	R_c (mL min^{-1})		ω_{ao} (kg kg^{-1})		T_{ao} (^{o}C)		T_{wo} (^{o}C)	
		High	Low	High	Low	High	Low	High	Low
Coefficient of determination	$R^2=\frac{[\sum_{i=1}^{n}(P_i-\bar{P})(M_i-\bar{M})]^2}{\sum_{i=1}^{n}(P_i-\bar{P})^2\sum_{i=1}^{n}(M_i-\bar{M})^2}$	0.85	0.94	0.99	0.96	0.92	0.92	0.98	0.98
Mean predictive error	$PE=\frac{1}{n}\sum_{i=1}^{n}(P_i-M_i)$	15.25	22.67	-0.00006	-0.00018	0.35	2.44	-0.33	-0.10
Mean absolute predictive error	$AE=\frac{1}{n}\sum_{i=1}^{n}\lvert P_i-M_i\rvert$	23.35	46.96	0.00010	0.00039	0.67	2.70	0.34	0.45
Root mean square error	$RMSE=\sqrt{\frac{1}{n}\sum_{i=1}^{n}(P_i-M_i)^2}$	49.42	80.67	0.00020	0.00067	0.99	4.04	0.44	0.70
Index of agreement	$IA=1-\frac{\sum_{i=1}^{n}(P_i-M_i)^2}{\sum_{i=1}^{n}(\lvert P_i-\bar{M}\rvert+\lvert M_i-\bar{M}\rvert)^2}$	0.96	0.98	1.00	0.99	0.92	0.86	0.98	0.99

Note: * where P is predicted values; M is measured values; $\bar{P}$ is mean predicted values; $\bar{M}$ is mean measured values, subscript p is for predicted quantities and subscript m is for measured quantities.

5.2 Temperature predictions

It appears that the simulation model slightly over-estimated the outlet air temperature (T_{ao}) but yet with an R^2 value of 0.92 at high and low air flowrates (Table 3). This over-estimation was more obvious with low air flowrate than with high air flowrate (Figure 6) which could be attributed to inaccuracy either related to the predicted T_{ao} or to the measured T_{ao}. Because the simulation was based on precise heat and mass balances and accurate input variables (i.e. T_{ai}, T_{wi}, m_a, ω_{ai}, and ω_{ao}), the difference between predicted and measured T_{ao} could be more due to errors in the measured T_{ao} rather than in the predicted T_{ao}. In order to verify this, a smoke trace test was conducted.

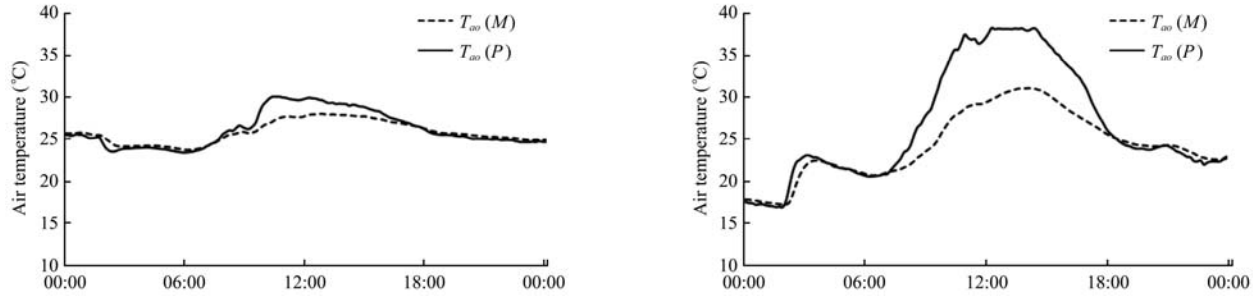

a. High air flowrate b. Low air flowrate

Figure 6 Measured (M) and predicted (P) outlet air temperature (T_{ao}) of the SWGH condenser at different air flowrate

Results showed that air was not moving in horizontal lines between the second humidifier and the condenser (Figure 7). The relatively hot seawater used to wet the second humidifier warmed up the higher air stream more than the lower air stream, giving it a tendency to move upwards. Furthermore, evaporation decreases as seawater flows downwards because water loses sensible heat due to evaporative cooling. This implies that air passing through the second humidifier at lower positions will be cooler and less humid than air at higher positions. Therefore, the temperature sensor placed at the outlet of the condenser was not measuring the temperature of the same air layer measured by the sensor placed at the inlet but rather the temperature of a cooler air layer, i.e. measured T_{ao} was cooler than the real temperature because of this phenomenon. Consequently, the small difference observed between the predicted and measured T_{ao} could be more attributed to inaccurate measurements related to the non-horizontal airflow pattern. This becomes evident when the difference between predicted and measured T_{ao} is compared at high and low air flowrates. Because the greenhouse fans exerted higher

suction at high air flowrate than at low flowrate, air stream was forced to move more horizontal (slightly deflected upwards) at high air flowrate compared to low flowrate. This explains why the measured T_{ao} was much closer to the predicted value at high flowrate than at low flowrate (Table 3). Having said that, the inaccuracy related to the simulation is still probable and further investigation is recommended.

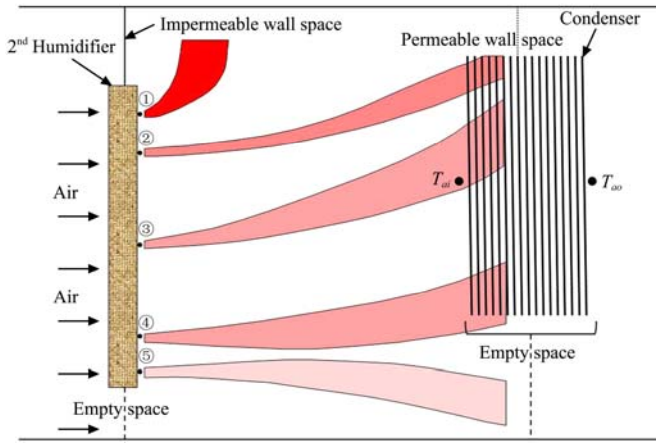

Figure 7 Observed air movement from the second humidifier to condenser using a smoke source placed at 5 vertical positions on the surface of the second humidifier

The accuracy of the model to predict the outlet seawater temperature (T_{wo}) was excellent with an R^2 of 0.98 for high and low air flowrates (Table 3). Figure 8 provides graphical comparisons between the predicted and measured T_{wo} for both flowrates.

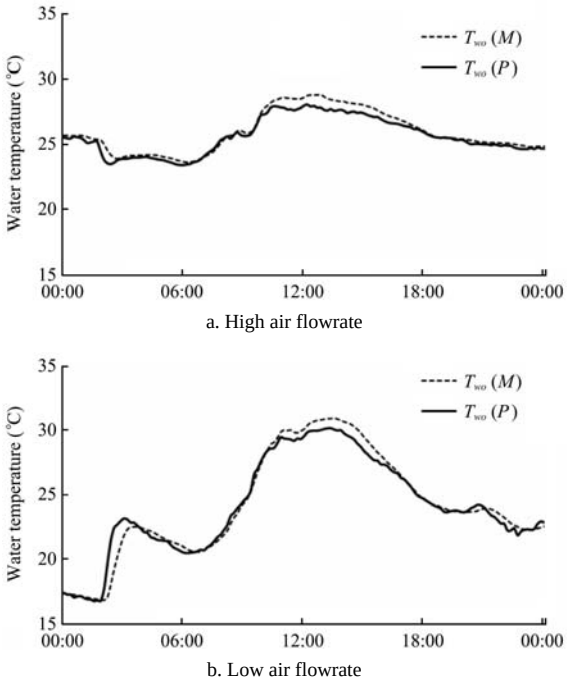

a. High air flowrate

b. Low air flowrate

Figure 8 Measured (M) and predicted (P) outlet seawater temperature (T_{wo}) of the SWGH condenser at different air flowrate

5.3 General remarks

It was observed from the experiments and simulation that the condenser of the SWGH produced more water at low air flow rate (303 L day^{-1}) than at high air flow rate (103 L day^{-1}) due to the increased time of contact between moist air and the condenser tubes which gave higher chance for condensation to take place at the low air flow rate. Therefore, it is recommended to run the greenhouse fans at low flowrates in order to attain more freshwater production. If it is necessary to ventilate the greenhouse at higher flowrates then some air should be allowed to bypass the second humidifier and the condenser to reduce the air flow, i.e. increasing condensation rate without affecting the crops cultivated in the greenhouse.

6 Conclusions

The simulation model presented in this study is capable in predicting four outlet parameters of the condenser in the SWGH in Oman using several climatic, operational and design input variables. The empirical relation developed to predict the condensation rate was accurate at high and low air flowrates (R^2 of 0.85 and 0.95, respectively). Using the predicted condensation rate, the model accurately predicted the outlet humidity ratio with R^2 of 0.99 and 0.96 at high and low air flowrates, respectively.

The accuracy of the model to predict the outlet air temperature was also excellent at high and low air flowrates (R^2 of 0.92). However, there were some occasions when the predicted outlet air temperature was slightly higher than the measured values. This discrepancy was either due to inaccuracy in measurements or simulation but with the aid of a smoke trace test, this error was more attributed to the inaccuracy of the measured outlet air temperature due to the non-horizontal air flow pattern. The accuracy of the model to predict the outlet seawater temperature was also very high (R^2 of 0.98) at high and low air flowrates.

Acknowledgement

The significant contribution of Dr. Osama Badr in the development of the model is highly appreciated. The first

author would like also to express his sincere gratitude to Mr. M. Al-Balushi for the technical assistance provided during the experimental work of this study. We would like also to extend our thanks to Dr. Mushtaque Ahmed for proofreading.

References

ABC. 2012. Sundrop Farms: ABC landline coverage. Available at: http://www.youtube.com/watch?v=KCup_B_RHM4. Accessed 12 September 2017.

Al-Ismaili, A. M. 2003. Modification of a quonset greenhouse to a humidification-dehumidification system: design, construction and pilot testing. M.S. thesis. Muscat, Oman: Sultan Qaboos University,.

Al-Ismaili, A. M. 2009. Modelling of a humidification-dehumidification greenhouse in Oman. Ph.D. diss., Ann Arbor, UK: Cranfield University.

Al-Ismaili, A. M., and H. Jayasuriya. 2016. Seawater greenhouse in oman: a sustainable technique for freshwater conservation and production. *Renewable and Sustainable Energy Reviews,* 54: 653–664.

Aljazeera-English. 2012. Sundrop Farms Aljazeera English Earthrise-series. Available at: http://www.youtube.com/watch?v=46Vzc8flmaQ. Accessed 12 September 2017

Alkhalidi, A., Y. Zurigat, B. Dawoud, T. Aldoss, and G. Theodordis. 2010. Performance of a greenhouse desalination condenser: An experimental study. In *1st International Nuclear and Renewable Energy Conference (INREC10)*, 1–7. Amman, 21 March

Bourouni, K., M. T. Chaibi, and A. Al-Taee. 2011. Water desalination by humidification and dehumidification of air, seawater greenhouse process. Available at: http://www.eolss.net/Eolss-sampleAllChapter.aspx. Accessed 12 September 2017.

Davies, P. A., and C. Paton. 2005. The seawater greenhouse in the United Arab Emirates: Thermal modelling and evaluation of design options. *Desalination,* 173(2): 103–111.

Davies, P. A., and C. Paton. 2006. The seawater greenhouse: background, theory and current status. *International Journal of Low-Carbon Technologies* ,1(2): 183–190.

Davies, P. A., K. Turner, and C. Paton. 2004. Potential of the seawater greenhouse in Middle Eastern climates. In *International Engineering Conference*, 523–540. Mutah, 26 April.

Davies, P., and C. Paton. 2004. The seawater greenhouse and the watermaker condenser. In *3rd International Heat Powered Cycles Conference*, 1–7. Larnaca, 11-13 October.

Dawoud, B., Y. H. Zurigat, B. Klitzing, T. Aldoss, and G. Theodoridis. 2006. On the possible techniques to cool the condenser of seawater greenhouses. *Desalination,* 195(1): 119–140.

Douani, M., T. Tahri, S. A. Abdul-Wahab, A. Bettahar, H. Al-Hinai, and Y. Al-Mulla. 2011. Modeling heat exchange in the condenser of a seawater greenhouse in oman. *Chemical Engineering Communications,* 198(12): 1579–1593.

Ghaffour, N., J. Bundschuh, H. Mahmoudi, and M. F. A. Goosen. 2015. Renewable energy-driven desalination technologies: A comprehensive review on challenges and potential applications of integrated systems. *Desalination,* 356:94–114.

Ghaffour, N., V. K. Reddy, and M. Abu-Arabi. 2011. Technology development and application of solar energy in desalination: MEDRC contribution. *Renewable and Sustainable Energy Reviews,* 15(9): 4410–4415.

Goosen, M. F. A., S. S. Sablani, C. Paton, J. Perret, A. Al-Nuaimi, I. Haffar, H. Al-Hinai, and W. H. Shayya. 2003. Solar energy desalination for arid coastal regions: development of a humidification–dehumidification seawater greenhouse. *Solar Energy,* 75(5): 413–419.

Goosen, M. F. A., S. S. Sablani, W.H. Shayya, C. Paton, and H. Al-Hinai. 2000. Thermodynamic and economic considerations in solar desalination. *Desalination,* 129(1): 63–89.

Grimson, E. D. 1937. Correlation and utilization of new data on flow resistance and heat transfer for cross flow of gases over tube banks. *Transactions of the ASME,* 59: 583–594.

Hajiamiri, M., and G. R. Salehi. 2013. Modeling of the seawater greenhouse systems. *Life Science Journal,* 10(8): 353–359.

Hausen, H. 1943. Darstellung des warmeuberganges in rohern durch verallgemeinerte potenzbeziehungen. *Z. VDI-Beiheft Verfahrenstechnic,* 4: 91–98.

Hausen, H. 1983. *Heat Transfer in Counter Flow, Parallel Flow and Cross Flow*. New York: McGraw-Hill.

Light-Works. 2001. Greenhouse designed with Simulink® revolutionizes agriculture in arid coastal regions. Available at: www.seawatergreenhouse.com. Accessed 7 May 2014.

Lovichit, W., C. Kubota, C. Y. Choi, and J. Schoonderbeek 2007. Greenhouse water recovery system for crop production in semi-arid climate. ASABE Paper No. 074012. Michigan: ASABE.

Perret, J. S., A. M. Al-Ismaili, and S. S. Sablani. 2005. Development of a humidification–dehumidification system in a quonset greenhouse for sustainable crop production in arid regions. *Biosystems Engineering,* 91(3): 349–359.

Quteishat, K., M. K. Abu Arabi, and K. V. Reddy. 2003. Review of MEDRC R&D projects. *Desalination,* 156(1-3): 1–20.

Raoueche, A., B. Bailey, and B. Stenning. 1996. Sensitivity analysis of the seawater greenhouse. In 22nd *WEDC Conference on reaching the unreached - Challenges for the 21st-Century*, 291-294. New Delhi, 9-13 September.

Sablani, S. S., M. F. A. Goosen, C. Paton, W. H. Shayya, and H. Al-Hinai. 2003. Simulation of fresh water production using a

humidification-dehumidification seawater greenhouse. *Desalination,* 159(3): 283–288.

Stanghellini, C., and W. T. van Meurs. 1992. Environmental control of greenhouse crop transpiration. *Journal of Agricultural Engineering Research,* 51: 297–311.

Tahri, T., S. A. Abdul-Wahab, A. Bettahar, M. Douani, H. Al-Hinai, and Y. Al-Mulla. 2009a. Simulation of the condenser of the seawater greenhouse: Part I: Theoretical development. *Journal of Thermal Analysis and Calorimetry,* 96(1): 35–42.

Tahri, T., S. A. Abdul-Wahab, A. Bettahar, M. Douani, H. Al-Hinai, and Y. Al-Mulla. 2009b. Simulation of the condenser of the seawater greenhouse: Part II: Application of the developed theoretical model. *Journal of Thermal Analysis and Calorimetry,* 96(1): 43–47.

Tahri, T., A. Bettahar, M. Douani, S. A. Abdul-Wahab, H. Al-Hinai, and Y. Al-Mulla. 2010. Solar desalination of seawater in a green-house: Simulating the effects of condensation and operating parameters (French). In *VIèmes Journées d'Etudes Techniques*, page. Marrakech, 5-7 May.

Tahri, T., M. Douani, S. A. Abdul-Wahab, M. Amoura, and A. Bettahar. 2013. Simulation of the vapor mixture condensation in the condenser of seawater greenhouse using two models. *Desalination,* 317: 152–159.

Tahri, T., M. Douani, M. Amoura, and A. Bettahar. 2016. Study of influence of operational parameters on the mass condensate flux in the condenser of seawater greenhouse at Muscat, Oman. *Desalination and Water Treatment*, 57(30): 13930–13937.

Yetilmezsoy, K., and S. A. Abdul-Wahab. 2014. A composite desirability function-based modeling approach in predicting mass condensate flux of condenser in seawater greenhouse. *Desalination,* 344: 171–180.

Zamen, M., M. Amidpour, and M. Rezaei Firoozjaei. 2013. A novel integrated system for fresh water production in greenhouse: Dynamic simulation. *Desalination,* 322: 52–59.

Zurigat, Y., T. Aldoss, B. Dawoud, and G. Theodordis. 2008. Greenhouse-State of the art review and performance evaluation of dehumidifier. *MEDRC Project*.

Nomenclature

symbol	
A	surface area, m^2
C_p	specific heat, J kg^{-1} $^oC^{-1}$
D	diameter of condenser tube, m
f_a	arrangement factor
h	specific enthalpy, kJ kg^{-1}
H	height of condenser tubes, m
k	thermal conductivity, W m^{-1} $^oC^{-1}$
L	length of condenser tubes, m
L_v	latent heat of vaporization at 0^oC, J kg^{-1}
m	mass flow rate, kg s^{-1}
Nu	Nusselt number
Pr	Prandtl number
Q	heat transfer rate, W
R_c	condensation rate, mL min^{-1}
Re	Reynolds number
S	spacing between adjacent tubes of the condenser, m
T	temperature, ^oC
	humidity ratio, kg kg^{-1}

Subscripts	
a	air, at air temperature
ai	air inlet value
ao	air outlet value
avg	average value
cd	conductive transfer
cv	convective transfer
D	diagonal
da	dry air
es	external surface
ext	external
int	internal
is	internal surface
L	parallel to the direction of flow
max	maximum
tube	condenser tube
T	transverse
w	seawater
wi	seawater inlet value
wo	seawater outlet value
wv	water vapour